

We are IntechOpen, the world's leading publisher of Open Access books Built by scientists, for scientists

6,900

Open access books available

186,000

International authors and editors

200M

Downloads

Our authors are among the

154

Countries delivered to

TOP 1%

most cited scientists

12.2%

Contributors from top 500 universities



WEB OF SCIENCE™

Selection of our books indexed in the Book Citation Index
in Web of Science™ Core Collection (BKCI)

Interested in publishing with us?
Contact book.department@intechopen.com

Numbers displayed above are based on latest data collected.
For more information visit www.intechopen.com



Detection and Avoidance Scheme for DS-UWB System: A Step Towards Cognitive Radio

Shaoyi Xu¹ and Rumin Yang²

¹Beijing Jiaotong University

²Chongqing University of Technology
P. R. China

1. Introduction

Cognitive radio (CR) improves spectrum efficiency to satisfy increasing demands on wireless transmission by dynamic spectrum access without interfering with legacy networks. In 2004, IEEE 802.22 Working Group was formed to develop a standard for wireless regional area networks (WRANs) based on CR technology (Hu et al et al., 2007). It is expected to obtain a broadband access to data networks on the vacant TV channels while avoiding harmful interference to licensed TV broadcasting in rural areas within a typical radius of 17km to 30km (Stevenson et al., 2006).

Ultra wideband radio (UWB), a promising technology, has found a myriad of exciting applications as well as generating a great deal of controversy, for its extremely broad bandwidth transmission as well as its revolutionary way of overlaying coexistent RF systems could cause interference on them (Lansford, 2004; Parr et al., 2003). Over the years, the co-existence problem of UWB has been all along a hot topic in the academy, industry, and regulatory bodies. After years of public debates, arguments, and comments, two important solutions to the co-existence problem are made—the policy-based power emission mask (FCC, 2002) and the device-centric cognitive radio (Lansford, 2004; Walko, 2005; Haykin, 2005). So far, several cognitive UWB schemes have been proposed, among which are soft-spectrum (Zhang & Kohno, 2003) scheme and detection-and-avoidance (DAA) scheme (Kohno & Takizawa, 2006).

Reliably detecting of weak primary signals is an essential functionality for a DAA UWB system as soon as a primary user (PU) comes back into operation on the operating channels. Two types of primary users are defined in a WRAN which are TV services and wireless microphones (WMs). Compared with TV services, it is tougher to detect WM signals for the following two reasons. Firstly, wireless microphones are low power devices and occupy a narrow bandwidth. The transmission power of a WM is as low as 50mW in a 200kHz bandwidth. When the sensor is several hundred meters away from this WM signal, the received signal-to-noise ratio (SNR) may be below -20dB (Zeng & Liang, 2007). Another, they utilize arbitrary unused TV bands and are deployed for a short time such that it is difficult for CR users to obtain much information on WM signals (De & Liang, 2007; Dhillon & Brown, 2008).

This chapter will concern two questions. Firstly, how to detect the weak primary signals. Secondly, how to avoid such interference from the primary user and how to coexist with it.

To address the first problem, we consider detecting multiple WM signals in a WRAN when UWB users want to use this spectrum and propose a singular value decomposition (SVD) based algorithm. To verify the better performance by using the suggested approach, simulation results by comparing to the traditional methods will be shown. For the second concern, a pulse-shaping scheme under the limit of a power spectrum density algorithm will be proposed. In a cognitive environment, the re-design of pulses should be agile enough and easily reconfigurable. Furthermore, to avoid interfering with the primary system, the transmission power of UWB should be considered.

2. Detection of weak primary signals in a cognitive radio network

2.1 Basic assumptions and problem formulation

Several methods have been suggested to detect WM signals. In (Mossa & Jeoti, 2009), a cyclostationary filter is proposed to grasp the existence of WM signals and to estimate their frequency locations. Obviously, such database dependent methods can not adapt to the dynamic signal detection. (Lei & Chin, 2008; Wu et al., 2009) proposed beacon based methods for wireless microphones but these put the onus on many already-deployed incumbent wireless microphones. (Zeng & Liang, 2009; Unnikrishnan & Shellhammer, 2007) investigate the method based on eigenvalues of received data matrix when a WM signal is present but can not solve the multiple WM signals detection in a wideband cognitive network. To the best of our knowledge, the literature of wideband spectrum sensing for multiple WM signals is very limited. Actually, it is inevitable that multiple wireless microphones appeared simultaneously. Furthermore, performing wideband spectrum sensing can improve detection efficiency and maximize the opportunistic throughput (Quan et al., 2008). (Kalke, 2005) estimated that about 25,000 licensed wireless microphones are utilized by recording studios of TV broadcasters, organizers and performers in concerts and theatres, commentators in sports events, film production crews and government agencies. To avoid interfering to each other, these WM signals must operate in different center frequencies with enough guard bandwidth. To detect multiple WM signals in a wide bandwidth, (Lim et al., 2007) suggested to use a cyclostationary filter with a filterbank to detect every sub-channel which is divided from the wide sensing spectrum in advance. If a conventional energy detector is used, the sensing process has to include two steps: coarse sensing and fine sensing. The former step determines the presence of WM signals and the latter step is required to decide which channel is occupied (IEEE 802.22 working Group for WRAN, 2006). Obviously, the system complexity and sensing periods will be greatly increased by using traditional methods to sense WM signals in a wideband spectrum.

In our work, we propose a singular value decomposition based algorithm to detect multiple WM signals in a CR network which can sense a wideband channel consisting of multiple narrowband channels. After performing SVD on the received data matrix of a wideband spectrum, the presence of WM signals is detected by comparing the singular values with a prefixed threshold and the number of WM signals can be determined at the same time. Then, the WM signals are approximated and the center frequencies of these WM signals are estimated. Consequently, guard bandwidths will be set on the two sides of the primary WM signals and CR users can still work on the other spectra within the sensing bandwidth without interfering with the primary wireless microphone users. The detection threshold and probability of false alarm are derived and simulation results confirm that our method is very effective and robust to detect and estimate multiple WM signals in a wideband spectrum.

Consider a CR network with N samples utilized to perform spectrum sensing at the i th CR user. Then the received signals at this CR user have two hypotheses as

$$\begin{cases} H_0 : & r_i(n) = u_i(n) \\ H_1 : & r_i(n) = h_i s_i(n) + u_i(n) \end{cases} \quad (1)$$

Here H_0 and H_1 respectively mean the primary user is inactive and the licensed user is operating. h_i is the channel gain between the PU and the i th secondary user. s_i represents the received PU signals by the i th SU and u_i is AWGN with zero mean and variance σ_u^2 , respectively. The test statistic for an energy detector is given by

$$T_i = \frac{1}{N} \sum_{n=1}^N |r_i(n)|^2 \quad (2)$$

Under the hypothesis H_0 , it shows a Gaussian random distribution when N is large with mean σ_u^2 and variance $\frac{2}{N} \sigma_u^4$. Hence, for a given probability of false alarm P_f , the threshold η of an energy detector can be derived as

$$\eta = \sigma_u^2 \left(1 + \frac{\sqrt{2} Q^{-1}(P_f)}{\sqrt{N}} \right) \quad (3)$$

where $Q(x) = (1 / \sqrt{2\pi}) \int_x^\infty e^{-t^2/2} dt$ is the normal Q-function.

In (Unnikrishnan & Shellhammer), it is pointed out that most wireless microphones use analog frequency modulation (FM) and a WM signal occupies only 200kHz. Specifically, most energy of a WM signal is contained in an only 40kHz bandwidth (Notor, 2006). However, IEEE 802.22 draft requires the sensing spectrum is at least one channel (6, 7 or 8MHz), and hence the proportion which a WM signal occupies is below 3%. Based on the above analysis, $s(t)$ can be modeled as a summation of multiple single-tone cosinoidal signals as

$$s(t) = \sum_{k=1}^P A_k \cos(2\pi f_k t + \theta_k) \quad (4)$$

where A_k , f_k and θ_k respectively denote the amplitude, center frequency and phase of the k th WM signal and P is the number of WM signals in the sensing spectrum. θ_k can be modeled as a uniform random variable over $[0, 2\pi)$. Without loss of generality, we assume s_i and u_i are independent of each other and $SNR = \frac{P_{WM}}{2\sigma_u^2}$ denotes the SNR of the primary WM signals received by the i th CR user where P_{WM} is the total power of P WM signals.

In this chapter, we consider that there are multiple WM signals in several sensing channels and each channel is a TV channel with 6MHz bandwidth. Under this assumption, we focus the detection of multiple WM signals on a wideband spectrum.

2.2 SVD based approach to detect and estimate multiple WM signals

In this section, we will present the SVD based method to detect the presence of WM signals and to estimate the number and center frequencies of these detected WM signals.

2.2.1 Technology to detect multiple WM signals

SVD plays an important role in signal processing and statistics, particularly in the area of linear systems. For a time series $r(n)$ with $n = 1, 2, \dots, N$, commonly, we can construct a Hankel matrix with $M = N - L + 1$ rows and L columns illustrated as follows:

$$\mathbf{R} = \begin{bmatrix} r(1) & r(2) & \dots & r(L) \\ r(2) & r(3) & \dots & r(L+1) \\ \vdots & \vdots & \ddots & \vdots \\ r(N-L+1) & r(N-L+2) & \dots & r(N) \end{bmatrix} \quad (5)$$

then \mathbf{R} is an $M \times L$ matrix. Its elements can be found by substitution of $r(n)$

$$\mathbf{R}_{ml} = r(m+l-1), \quad m = 1, 2, \dots, M \text{ and } l = 1, 2, \dots, L. \quad (6)$$

Using the SVD, \mathbf{R} can be factorized as

$$\mathbf{R} = \mathbf{U}\mathbf{\Sigma}\mathbf{V}^H \quad (7)$$

where \mathbf{U} and \mathbf{V} are an $M \times M$ and an $L \times L$ unitary matrix, respectively. The columns of \mathbf{U} and \mathbf{V} are called left and right singular vectors, respectively. $\mathbf{\Sigma} = \text{diag}(\lambda_1, \lambda_2, \dots, \lambda_m)$ is a diagonal matrix whose nonnegative entries are the square roots of the positive eigenvalues of $\mathbf{R}^H\mathbf{R}$ or $\mathbf{R}\mathbf{R}^H$. These nonnegative entries are called the singular values of \mathbf{R} and they are arranged in a decreasing order with the largest one in the upper left-hand corner. $[\]^H$ denotes the complex transpose of a matrix.

When no any primary WM signal is present, the received signal $r(n)$ includes only AWGN contribution such that its singular values are similar and close to zero. When WM signals are active whose power is higher than a threshold, there will exist several dominant singular values to represent these WM signals. As a result, the WM signals can be detected by examining the presence of dominant singular values.

It is critical to determine the number of WM signals P and we will present such method in the following part. To simplify our analysis, we assume that the power values of all WM signals received in the detected spectrum are approximately same, that is to say $A_1 \approx A_2 \approx \dots \approx A_P$. Since the SNR of primary WM signals received by the secondary detectors is usually very weak, we think this assumption is feasible. Several methods can be utilized to determine if the dominant singular values are present. It is pointed out in (Teh et al, 1995) that the relationship between the number of dominant singular values K and the number of single-tone cosinoidal signals P has the form as $K = 2P$, therefore, threshold γ can be adopted which is the ratio between the first singular value and the $(2X+1)$ th singular value. That is to say, if the following equation is true, P WM signals can be declared to be present as

$$\text{If } \lambda_1 / \lambda_{2X+1} \geq \gamma, \text{ then } P = X \quad (8)$$

and the expression of γ will be derived in Section 2.3.

2.2.2 Technology to estimate the center frequencies of multiple WM signals

Once WM signals are detected to be active in the sensing channels, the center frequencies of these primary WM signals need to be estimated such that a guard bandwidth can be

retained and CR users utilize the other spectra to improve spectrum efficiency. Next, we will present the frequency estimation technique by using SVD.

After P WM signals are detected to be active, the data matrix \mathbf{R} in (5) is the superposition of the WM signal space and AWGN space and \mathbf{R} can be partitioned into two subspaces as follows

$$\begin{aligned} \mathbf{R} &= \mathbf{U}\mathbf{\Sigma}\mathbf{V}^H = [\mathbf{U}_S \quad \mathbf{U}_U] \begin{bmatrix} \mathbf{\Sigma}_S & 0 \\ 0 & \mathbf{\Sigma}_U \end{bmatrix} [\mathbf{V}_S \quad \mathbf{V}_U]^H \\ &= \mathbf{U}_S\mathbf{\Sigma}_S\mathbf{V}_S^H + \mathbf{U}_U\mathbf{\Sigma}_U\mathbf{V}_U^H = \mathbf{R}_S + \mathbf{R}_U \end{aligned} \tag{9}$$

where

$$\mathbf{\Sigma}_S = \text{diag}(\lambda_1, \lambda_2, \dots, \lambda_{2P}), \tag{10}$$

and

$$\mathbf{\Sigma}_U = \text{diag}(\lambda_{2P+1}, \lambda_{2P+2}, \dots, \lambda_m) \tag{11}$$

with $\lambda_1 > \lambda_2 > \dots > \lambda_{2P} \gg \lambda_{2P+1} > \lambda_{2P+2} > \dots > \lambda_m$ corresponding to the singular values in the WM signal subspace and the noise subspace, respectively. $\lambda_1, \lambda_2, \dots, \lambda_{2P}$ are $2P$ dominant singular values which correspond to the P WM signals. $\mathbf{R}_S = \mathbf{U}_S\mathbf{\Sigma}_S\mathbf{V}_S^H$ and $\mathbf{R}_U = \mathbf{U}_U\mathbf{\Sigma}_U\mathbf{V}_U^H$ are the WM signals subspace and the noise subspace, respectively. By rearranging \mathbf{R}_S into a time serial, we can get the estimated data vector of WM signals $\mathbf{y} = [y_1, y_2, \dots, y_N]^T$ which includes P WM signals. Next, we will present the algorithm to estimate P center frequencies corresponding to P WM signals.

We define $\mathbf{Y} = FFT(\mathbf{y}) = [Y_1, Y_2, \dots, Y_N]^T$ as the N -point Fast Fourier Transform (FFT) operation so we can use the theory of the Rife and Boorstyn (Rife & Boorstyn, 1974) as the frequency estimation of the WM signal which has the maximum power

$$k_{1_max} = \max^{-1}[|\mathbf{Y}[k]|], \quad 1 \leq k \leq N \tag{12}$$

$$\hat{f}_1 = \frac{k_{1_max}}{N} f_s \tag{13}$$

where $|\cdot|$ is the absolute value operator, $\max(\cdot)$ operator means k_{1_max} is the k_1 th sampling point where $|\mathbf{Y}[k]|$ obtains its maximum and f_s is the sampling frequency.

By applying equation (12) and (13), the center frequency of the WM signal which has the maximum power can be acquired. Following the similar step, we can obtain the approximate center frequency for the j th WM signal as

$$k_{j_max} = \max^{-j}[|\mathbf{Y}[k]|], \quad 1 \leq k \leq N \tag{14}$$

and

$$\hat{f}_j = \frac{k_{j_max}}{N} f_s \tag{15}$$

where k_{j_max} presents the k_j th sampling point corresponding to j th peak magnitude.

From the above analysis it can be concluded that this estimation algorithm is easy to implement since only FFT is required. By using FFT, the efficiency of frequency estimation can be improved greatly. Another, the inaccurate knowledge of P will not affect frequency estimation. If P is under or over estimated, then fewer or more frequencies will be estimated than the true number.

Rife and Boorstyn pointed out that when SNR is high enough, the true frequency has a high probability lies in the range (Rife & Boorstyn, 1974)

$$f \in [\hat{f} - (f_s / 2N), \hat{f} + (f_s / 2N)]. \quad (16)$$

In summary, the SVD based detection and estimation algorithm consists of the following steps:

- Step 1.** Pick a number L so that $k < L < N - k$ (Tufts & Kumaresan, 1982), where N is the number of sampling points and k is the number of dominant singular values. In our work, $k = 2P$.
- Step 2.** Arrange the received signal vector \mathbf{r} to form a Hankel data matrix \mathbf{R} as (5). Then compute the SVD of \mathbf{R} and obtain all singular values of \mathbf{R} .
- Step 3.** Calculate the threshold $\gamma = \lambda_1 / \lambda_{2X+1}$ ($X = 1, 2, \dots$) and compare the ratio $\lambda_1 / \lambda_{2X+1}$ with the predefined threshold γ . If $\lambda_1 / \lambda_{2X+1} \geq \gamma$, the WM signals are determined to be present and the number of WM signals can be derived by $P = X$. Otherwise, no WM signal is declared to be active. The derivation of γ will be explained in Section 2.3.
- Step 4.** If P WM signals are declared to be present, compute \mathbf{R}_S then arrange it into a data vector \mathbf{y} . Apply FFT on \mathbf{y} and consecutively find the number of the point k_{j_max} at which the k_j th peak amplitude of the FFT is approached.
- Step 5.** Obtain the estimated center frequency of j th WM signal by using (12 –15).

2.3 Theoretical analysis and determination of threshold

In this section, we will derive the threshold γ and probability of false alarm P_f .

We denote \mathbf{R}_S ($M \times L$) and \mathbf{R}_U ($M \times L$) as the Hankel matrix of WM signals and an AWGN signal, respectively, such that $\mathbf{R}_U \sim N_p(0, \mathbf{\Sigma})$ where p is the dimension of \mathbf{R}_U and $\mathbf{\Sigma}$ is the covariance matrix. Since the power of WM signals is usually very low, the distribution of $\mathbf{R}_S + \mathbf{R}_U$ can be approximated as $N_p(0, \mathbf{\Sigma})$. According to (Zeng & Liang, 2009; Johnstone, 2001), we have the following three theorems:

Theorem 1. Assume $M/L \geq 1$ and N is large enough, the largest singular value can be approximated as

$$\lambda_1 \approx \sqrt{\frac{\sigma_u^2}{N} (\sqrt{N} + \sqrt{ML})^2}. \quad (17)$$

Theorem 2. Assume $M/L \geq 1$ and N is large enough, the largest singular value follows the following distribution

$$\frac{\lambda_1^2 - \mu_{ML}}{\delta_{ML}} \sim F_1 \quad (18)$$

where μ and δ are called a center constant and a scaling constant and they are defined as

$$\mu_{ML} = (\sqrt{M-1} + \sqrt{L})^2 \tag{19}$$

and

$$\delta_{ML} = (\sqrt{M-1} + \sqrt{L}) \left(\frac{1}{\sqrt{M-1}} + \frac{1}{\sqrt{L}} \right)^{\frac{1}{3}}. \tag{20}$$

F_1 is the distribution function of Tracy-Widom distribution of order 1 which has the form as

$$F_1(s) = \exp \left\{ -\frac{1}{2} \int_s^\infty q(x) + (x-s)q^2(x) dx \right\}, s \in \mathbb{R} \tag{21}$$

and q solves the Painlevé II differential function (Johnstone, 2001).

Theorem 3. The distribution of r th largest singular value ($r < L$) has the approximate distribution as

$$\Phi(\lambda_{r+1}^2 | M, L, \Sigma) \approx \Phi(\lambda_1^2 | M, L-r, I_{L-r}) - c_{M,L} \tag{22}$$

where $c_{M,L}$ is an empirical constant.

Based on the above three theorems, as a result, P_f can be presented as

$$\begin{aligned} P_f &= P(\lambda_1 / \lambda_{2X+1} < \gamma) = P(\lambda_1^2 / \lambda_{2X+1}^2 < \gamma^2) \\ &= P(\lambda_{2X+1}^2 / \lambda_1^2 > 1 / \gamma^2) = P(\lambda_{2X+1}^2 > \lambda_1^2 / \gamma^2) \\ &\approx P\left(\lambda_{2X+1}^2 > \frac{\sigma_u^2}{\gamma^2 N} (\sqrt{N} + \sqrt{ML})^2\right) \\ &= 1 - \Phi\left(\lambda_{2X+1}^2 > \frac{\sigma_u^2}{\gamma^2 N} (\sqrt{N} + \sqrt{ML})^2 \mid M, L, \Sigma\right) \\ &\approx 1 - \Phi\left(\lambda_1^2 > \frac{\sigma_u^2}{\gamma^2 N} (\sqrt{N} + \sqrt{ML})^2 \mid M, L-2X, I_{L-2X}\right) + c_{M,L} \\ &= 1 - F_1\left(\frac{\frac{\sigma_u^2}{\gamma^2 N} (\sqrt{N} + \sqrt{ML})^2 - \mu_{M,L-2X}}{\delta_{M,L-2X}}\right) + c_{M,L} \end{aligned} \tag{23}$$

Hence, for a pre-determined P_f , the required threshold γ can be represented as

$$\gamma = \frac{\sigma_u (\sqrt{N} + \sqrt{ML})}{\sqrt{N \left[\delta_{M,L-2X} F_1^{-1}(1 + c_{M,L} - p_f) + \mu_{M,L-2X} \right]}}. \tag{24}$$

2.4 Simulation results

2.4.1 Simulation parameters

Since it is difficult to derive the accurate closed form expression of γ and P_f , we need to resort to simulations for evaluating the performance of our approach.

We consider the spectrum of interest is three consecutive channels which means the sensing bandwidth is 18MHz. We assume that three WM signals are distributed on this 18MHz bandwidth and their SNRs are same. The signals are firstly down-converted into baseband and filtered by a baseband filter with bandwidth 18MHz. And then, these WM signals have the center frequency of 2.4MHz, 8MHz and 14.2MHz, respectively. The selected sampling frequency f_s must be larger than the Nyquist frequency of the WM signal which has the highest center frequency and in our simulation f_s should be larger than 28.4MHz. To find the threshold γ , we require the probability of false alarm is $P_f = 0.1$. To evaluate the performance of frequency estimation, we define the mean estimation precision for the frequency estimation as

$$\varepsilon = \frac{\sum_{j=1}^3 \frac{|\hat{f}_j - f_j|}{f_j}}{3}. \quad (25)$$

where \hat{f}_j and f_j are the estimated j th center frequency and the j th ($j \leq 3$) true center frequency, respectively. To investigate our proposal, we compare our simulation results with a conventional energy detector whose threshold has been given in (3).

It has been shown in (Tufts & Kumaresan, 1982) that when the column number L in a Hankel matrix satisfies the inequality $2P < L < N - 2P$, we can obtain the correct or approximately correct estimation result. However, to the best of our knowledge, it has not been seen that the optimal L theoretically, moreover, the optimal L is different in different cases. In our work, the simulation results show that satisfying $2P < L < N - 2P$, different L has no significant impact on the system performance and frequency estimation.

In our work, without specific explanation, the sampling frequency is selected as $f_s = 36$ MHz and we select $L = N/5$ as the column number in our following simulations.

2.4.2 Simulation results and analysis

Fig. 1 shows simulation results of the probability of detection (P_d) vs. SNR when the proposed SVD based method and a classical energy detector are used. To investigate the effect for different WM signals, we show simulation results for the single WM signal with a center frequency of 2.4MHz and multiple WM signals, respectively. From this figure we can conclude that the detection performance can be improved greatly by using our method, especially for the single WM signal. For example, for the target P_d of 90%, a 4dB improvement can be obtained than an conventional energy detector by using the proposed approach for a single WM signal. For the multiple WM signals, an improvement of 2dB can be attained compared with the conventional energy detector. To evaluate the performance of the detector, the receiver operating characteristic (ROC) curves are illustrated in Fig. 2 when SNR is -12dB for the single WM signal and SNR = -10dB for three primary WM signals. We plot the P_d under H_1 against P_f under H_0 when P_f changes from 0.001 to the desired 0.1. We can observe that the ROC curve of our algorithm is much higher than that of the energy detector for both the single WM signal and multiple WM signals which verifies the better performance of our detector.

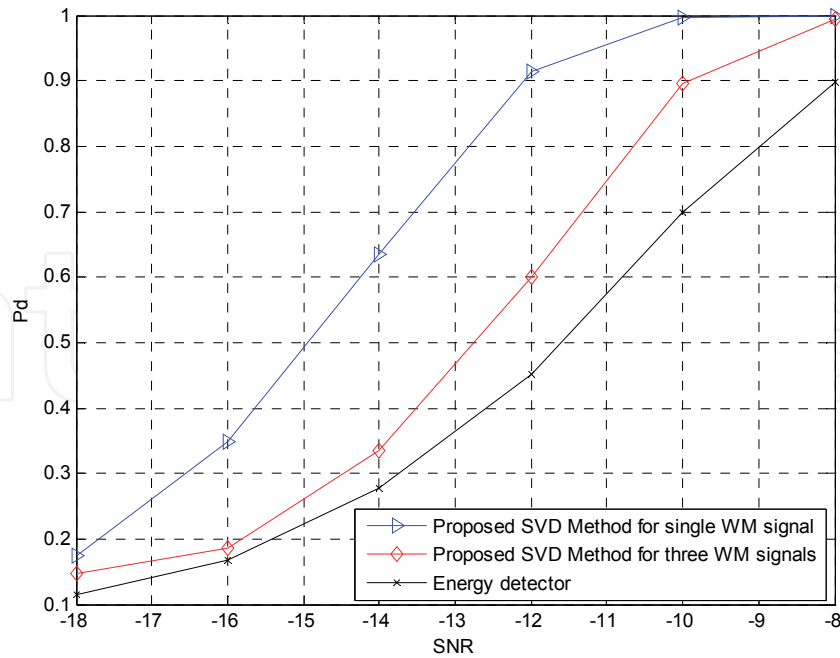


Fig. 1. Comparison of P_d between the proposed SVD-based method and a energy detector when PU is a single WM signal and three WM signals.

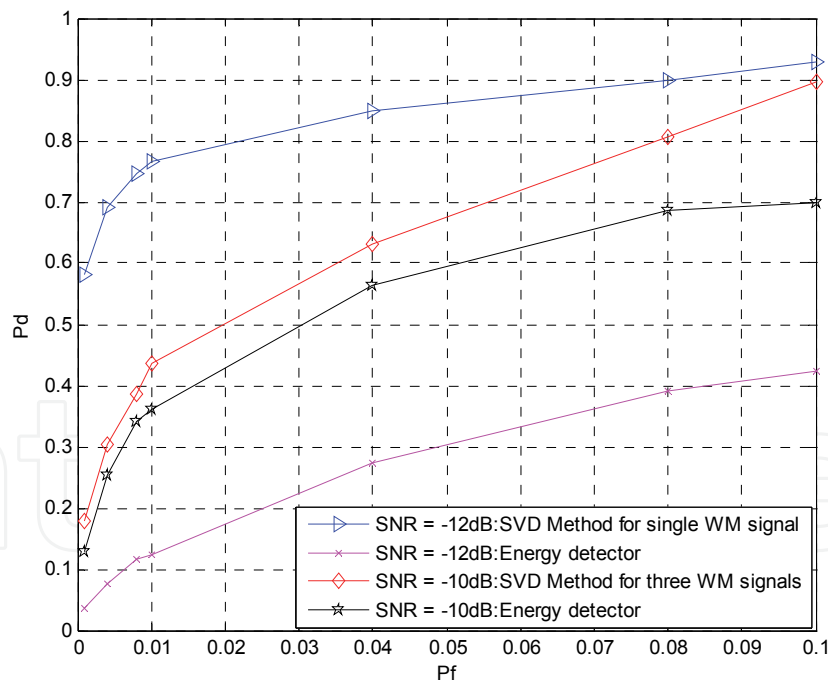


Fig. 2. Comparison of ROC curve between the SVD-based method and an energy detector when PU is a single WM signal and three WM signals.

To study the robustness of our algorithm, we first compare the P_d of our SVD based detection method under different column number L when three primary WM users operate simultaneously. Fig. 3 depicts the simulation results when $L = 3N/4, N/2, N/3$ and $N/5$, respectively. From this figure we can observe that although different L is taken, a good

detection probability can be achieved with very slight difference. Then, we compare the P_d of the proposed approach under different sampling frequency f_s . The used sampling frequencies are 24MHz, 30MHz, 36MHz and 48MHz, respectively. Among these frequencies, 24MHz is lower than the Nyquist frequency of the WM signal whose center frequency is 14.2MHz. From Fig. 4 we can conclude that with the changing of f_s , the probability of detection shows very slight difference. Even for the $f_s = 24$ MHz which is lower than the Nyquist frequency, a good P_d can be obtained which proves that our method is robust for different sampling frequency.

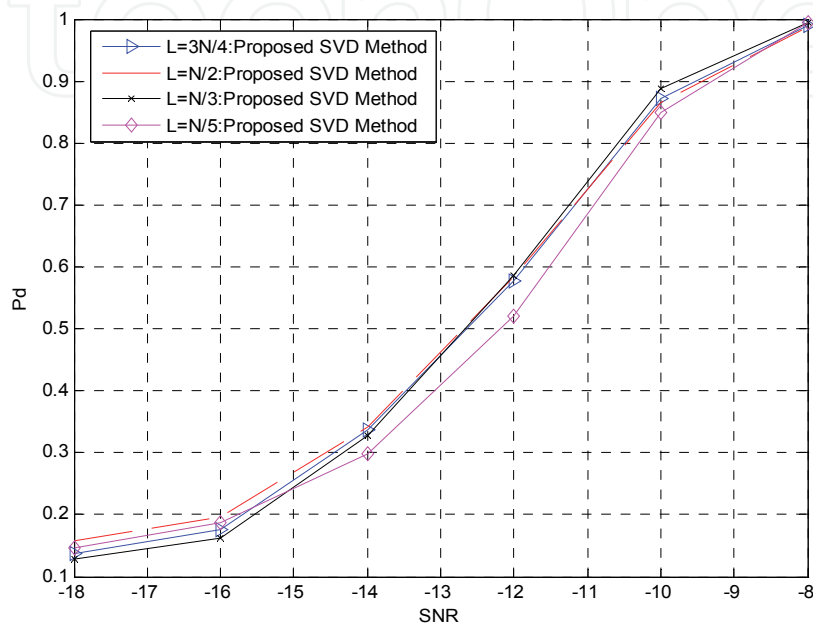


Fig. 3. P_d vs. SNR with different column number L for three WM signals.

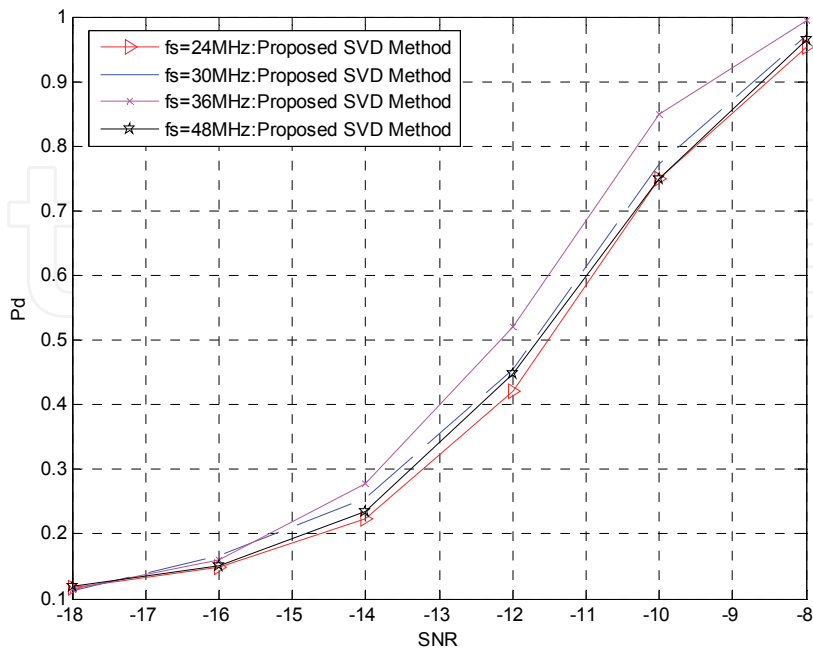


Fig. 4. P_d vs. SNR with different f_s for three WM signals.

To investigate the estimation performance of the WM's center frequency, we plot the mean estimation precision ε in Fig. 5 and 6 when L and f_s change. From these two figures we can see that the proposed frequency estimation method is very effective. For example, for the f_s of 36MHz and SNR = -10dB, the absolute error of the worst estimation is within 10kHz. Whereas, a nearly perfect frequency estimation can be obtained for $f_s = 36$ and 48MHz when SNR = -10dB. In Fig. 5, an obvious result can be found that ε gets better with the increase of f_s . This is feasible since it is more possible to find the j th magnitude when the sampling rate is larger. However, higher f_s means a higher requirement for the system complexity. As a result, a tradeoff is needed to consider between system complexity and a satisfying ε . Figure 5 also proves that the estimation precision can be degraded severely if a f_s lower than the Nyquist frequency is used. Fig. 6 presents the mean estimation precision ε when $f_s = 36$ MHz and $L = 3N/4, N/2, N/3$ and $N/5$, respectively. From Fig. 6 we can conclude that the difference of L has no significant impact on ε , especially when SNR is higher than -12dB.

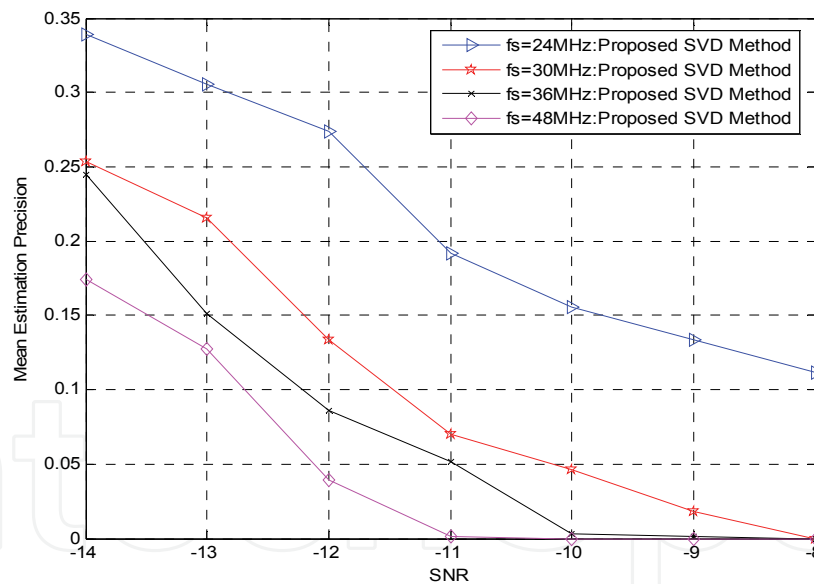


Fig. 5. Mean estimation precision of center frequency vs. SNR with different sampling frequency f_s for three WM signals.

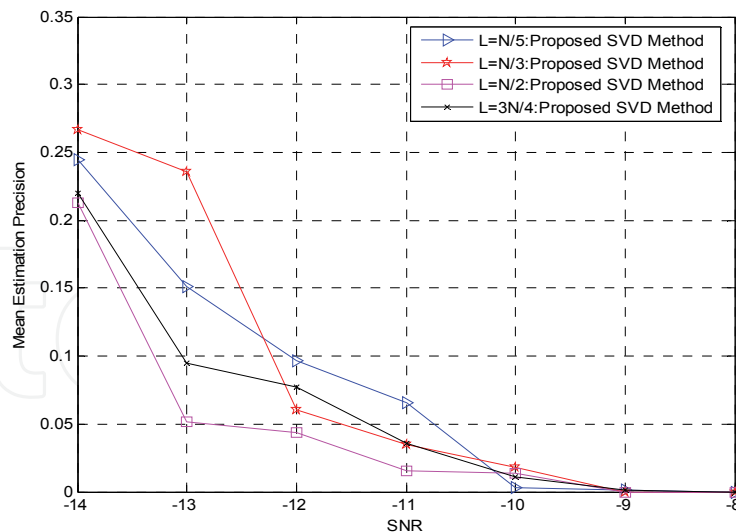


Fig. 6. Mean estimation precision of center frequency vs. SNR with different column number L for three WM signals.

2.5 Conclusions

In this part, we proposed a SVD based approach to detect and estimate multiple WM signals in a WRAN when a UWB system wants to use this spectrum. After performing SVD on the received data matrix, the presence and number of these WM signals can be detected and their center frequencies can be estimated. Consequently, guard bandwidths are retained to protect these primary users and the other detected spectra are available for the CR users. Simulation results prove that our method is simple and robust and it is especially suitable for detection and estimation of WM signals in a wideband spectrum sensing.

3. Detection and avoidance scheme based on orthonormal expansion

As well known, UWB technology is divided into two distinctive groups. The first group, known as multi-band UWB (MB-UWB), divides the entire UWB band into many sub-bands, with each sub-band being allocated a sinusoidal carrier. The DAA scheme mentioned above originates from this multi-band way of using UWB spectrum—each time a sub-band is detected being interfered, the carrier allocated for it is turned off. The second group is known as direct sequence UWB (DS-UWB), which, unlike the first, typically adopts a single-band transmission and depends entirely on varying pulse shapes to fit given spectrum masks; therefore, it is relatively difficult to turn on/off individual sub-band. A question is thus raised: Can the spectrum of the single-band DS-UWB be soft?

To answer this question, let us first investigate the currently proposed DS-UWB pulses: Rayleigh monocycle, Cubic monocycle, Gaussian monocycle, Gaussian doublet (Benedetto et al., 2006; Benedetto et al., 2004), high-order Gaussian derivatives (Win, 2000), modified Hermite polynomials (Ghavami et al., 2001) and so forth. The finding is somewhat discouraging—all of them feature fixed spectra. Used individually, they are not soft at all. Then, can the combinations of them be soft? As addressed in (Benedetto et al., 2004), a group of Gaussian derivatives have been linearly combined to generate an aggregate pulse that yields maximum spectral capacity. Such a combination adopts random-search optimization method, in the sense that a large number of combination coefficients are randomly

generated and the resulting combinations are evaluated. The combination that has minimum distance to the targeted spectrum mask is picked up as the optimal combination. This optimization method demands a huge number of iterations before finding the optimum. The converging time varies from situation to situation, so the linear combination methods are something between fixed and soft.

Moreover, cognitive UWB devices need to design and re-design the pulses on the scene of communication instead of having them preset or fixed in factories. In cognitive environment, the re-design of DS-UWB pulse must be agile enough and easily re-configurable.

To this end, we propose a soft-spectrum-based detection-and-avoidance algorithm for the single-band DS-UWB systems. The algorithm adopts a co-basis expansion method, in the sense that the well-known Hermite-Gaussian functions (HGFs) are used to constitute a common basis for both the time and frequency domains. The co-basis has twofold advantages: First, it yields the pulses directly from expanding the given soft-spectrum masks in frequency domain, so the pulses can conform to arbitrary spectrum masks. Second, the co-basis (that is, the HGFs) can be digitalized and built into matrices, such that whenever a new soft-spectrum is sensed or discovered, its expansion by the co-basis is as simple as matrix multiplications. As a result, the algorithm is really soft, low complex, always convergent, and agile enough for cognitive purpose.

3.1 The establishment of the soft-spectrum mask

The criterion for the design of DAA pulses is the ruling of the Federal Communications Commission (FCC), namely, the FCC's power emission mask (FCC, 2002), which ranges from 3.1 to 10.6GHz with power limit $P_{\max}=-41.3\text{dBm/MHz}$. Within the allocated UWB band, other radio systems such as IEEE 802.11a or HiperLan has already been in operation. For cognitive purpose, the DS-UWB radio must be aware of the existence of such primary systems before transmission and automatically avoid the frequency bands in use by primary users.

In the design of the DAA scheme for DS-UWB radio, our emphasis is placed on the side of avoidance. In order not to digress our focus, we leave the side of detection to reference to well-established spectral estimation methods in literature, for example, the multi-taper spectral estimator that performs fast Fourier transform (FFT) and threshold inspection (Haykin, 2005; Welch, 1967). Before transmission, the DS-UWB radio senses the ambient radio environment with a detecting unit. Upon detecting an in-use sub-band, it calculates the 10dB-bandwidth of the sub-band and marks the sub-band as forbidden. In a recursive manner, DS-UWB radio sweeps the entire UWB band and records all the forbidden sub-bands. After the sensing process is over, the UWB radio establishes a soft-spectrum model that conforms not only to the FCC mask but also to the real-time radio environment. The soft-spectrum model so-established can be expressed as

$$R_{ss}(f) = \begin{cases} P_{\max} & f \in I - I_s \\ 0 & f \in I_s \end{cases} \quad (26)$$

where $P_{\max}=-41.3\text{dBm/MHz}$, $I=[3.1\text{GHz}, 10.6\text{GHz}]$, and I_s represents the union of the forbidden sub-bands.

3.2 The relationship between the soft-spectrum and the frequency response

The DS-UWB radio is by nature a spread spectrum system, whose transmitted waveforms can be characterized as follows (Ye et al., 2004),

$$s(t) = \sum_{k=-\infty}^{\infty} \sum_{j=1}^{N_c} p(t - kT_b - jT_c) b_k c_p^j \quad (27)$$

where b_k is the k th data bit with duration T_b ; T_c is the chip duration; N_c is the spreading factor (that is, $T_b = N_c T_c$); c_p^j is the j th chip of the pseudorandom code; $p(t)$ is the pulse waveform. Through substitution of variables Eq. (27) can be simplified as:

$$s(t) = \sum_{i=-\infty}^{\infty} d_i p(t - iT_c) \quad (28)$$

where

$$i = kN_c + j \text{ and } d_i = d_{k,j} = c_p^j b_k \quad (29)$$

The autocorrelation function of $s(t)$ is given by (Proakis, 2003)

$$r_{ss}(\tau) = \frac{1}{T_c} \sum_{l=-\infty}^{\infty} r_{dd}(l) r_{pp}(\tau - lT_c) \quad (30)$$

where $r_{dd}(\bullet)$ represents the autocorrelation function of the information sequence $\{d_i \in \{\pm 1\}\}$; $r_{pp}(\bullet)$, the autocorrelation function of the pulse. Correspondingly, the PSD of $s(t)$ is given by

$$R_{ss}(f) = \frac{1}{T_c} R_{dd}(f) |P(f)|^2 \quad (31)$$

which indicates that the PSD of the transmitted waveforms depends not only on the frequency response of the pulse, $P(f)$, but also on the PSD of the information sequence, $R_{dd}(f)$, and on the chip duration T_c as well. However, since the sequence $\{d_i \in \{\pm 1\}\}$ can be viewed as an uncorrelated random process with zero mean and unitary variance (Benedetto et al., 2004; Ye et al., 2004), that is, $r_{dd}(l) = \delta(l)$, and $R_{dd}(f) = 1$, the autocorrelation function defined by Eq. (30) and the PSD defined by Eq. (31) can be further simplified respectively as follows,

$$r_{ss}(\tau) = \frac{1}{T_c} r_{pp}(\tau) = \frac{1}{T_c} \int_{-\infty}^{\infty} p(t) p^*(t + \tau) dt \quad (32)$$

and

$$R_{ss}(f) = \frac{1}{T_c} |P(f)|^2 \quad (33)$$

By substituting Eq. (26) into Eq. (33), we obtain the frequency response $P(f)$ of the transmitted DS-UWB waveforms that conforms both to the FCC mask and to the ambient RF environment, such $P(f)$ we refer to as soft-spectrum mask, namely

$$P(f) = \sqrt{T_c R_{ss}(f)} = \begin{cases} A & f \in I - I_s \\ 0 & f \in I_s \end{cases} \quad (34)$$

where

$$A = \sqrt{10^{P_{\max}/10} \times 10^{-9} \times T_c} \quad (\text{V/Hz}) \tag{35}$$

3.3 The establishment of a co-basis for both the time and frequency domain

The frequency response given by Eq. (34) is inherently an energy signal and can be uniquely expanded by orthonormal functions that span the signal base. But, an ordinary expansion does not suffice here. In the design of soft-spectrum-based DAA pulse, we need a common basis for both the time and frequency domains, that is, a co-basis. With this co-basis, the well-known orthonormal expansion method will do wonders for the design of pulses, yielding the waveform of the pulses (time domain) by expanding the soft-spectrum in the frequency domain.

Hermite-Gaussian functions (HGFs) constitute ideally such a co-basis.

The HGFs are combinations of Hermite polynomials with a Gaussian function, as written as follows (Ozaktas et al., 2000),

$$\varphi_l(u) = a_l H_l(\sqrt{2\pi} u) e^{-\pi u^2}, \quad a_l = 2^{1/4} / \sqrt{2^l l!} \tag{36}$$

where $H_l(\bullet)$ denotes the l th order Hermite polynomial. The generation function for Eq. (36) is

$$\varphi_l(u) = \frac{(-1)^l a_l}{(\sqrt{2\pi})^l} e^{\pi u^2} \frac{d^l}{du^l} e^{-2\pi u^2}, \quad l = 0, 1, 2, \dots \tag{37}$$

Note that the HGFs defined by Eqs. (36) and (37) are slightly different from those defined in classical mathematical textbooks – here, they are $\sqrt{2\pi}$ -scaled, so that they turn out to be the eigenfunctions of fractional Fourier transform (Ozaktas et al., 2000). In other words, because the HGFs are $\sqrt{2\pi}$ -scaled, they are shape-invariant to fractional Fourier transform (Ozaktas et al., 2000), that is,

$$F^\alpha \{ \varphi_l(u) \} = e^{-i\alpha l\pi/2} \varphi_l(\mu) \tag{38}$$

where F^α denotes fractional Fourier transform (FRFT) operator; $e^{-i\alpha l\pi/2}$, the corresponding eigenvalues; α , the order of the FRFT.

The FRFT is a generalization of the ordinary Fourier transform with an order parameter α . The α -th order fractional Fourier transform is the α -th power of the ordinary Fourier transform operation. When $\alpha = -1$, the corresponding FRFT operation is exactly the ordinary inverse Fourier transform. Under such circumstance, Eq. (38) becomes

$$F^{-1} \{ \varphi_l(u) \} = i^l \varphi_l(\mu) \tag{39}$$

which indicates that the HGFs are shape-invariant to the inverse Fourier transform except for a phase shift. This nice property makes the HGFs constitute a common basis for both the frequency and time domain. To emphasize this, we introduce two normalized variables u and μ in place of the natural frequency f and time t . The relationship among them will be addressed later on.

3.4 The dimension of the co-basis

Before proceeding, we need to determine the dimension of the co-basis, M , or equivalently, the number of HGFs involved in the expansion. Mathematically, the orthonormal expansion is least-mean-square approximation to the signal being expanded (Proakis, 2003), as stated as follows,

$$Q = \int_{-\infty}^{\infty} [P(f) - \sum_{l=0}^{M-1} c_l \phi_l(f)]^2 df = \int_{-\infty}^{\infty} P^2(f) df - \sum_{l=0}^{M-1} c_l^2 \quad (40)$$

where the square error Q manifests itself as in-band and out-of-band ripples in the expansion of the signal. In the case that the magnitude of the ripples is specified, Q can be computed according to the specifications and then M is obtained by solving Eq. (40). In other cases that the ripples are not of major concern, as in the current DAA case, M can be determined by rule of thumbs. For example, it has been verified by computer simulations that a medium M between 30 and 100 is sufficient for performing DAA functionalities that avoid two to four sub-bands.

3.5 The representation of the soft-spectrum mask by the co-basis

After determining the number of HGFs participating in the expansion, we need next to normalize the natural frequency argument of the soft-spectrum mask as given by Eq. (34). The purpose of such normalization is to let the support of the soft-spectrum mask match the support of the co-basis. The support of the co-basis is not compact, but its energy is mostly (say 90%) concentrated on a finite interval (Ozaktas et al., 2000) $[-u_H, u_H]$, where

$$u_H = \left\lceil \sqrt{\frac{(M+0.5)}{\pi}} \right\rceil \quad (41)$$

where $\lceil \cdot \rceil$ means rounding up to the nearest integer. u_H is closely related to the dimension of the co-basis and is used to determine a scaling factor τ ,

$$\tau = \frac{u_H}{f_H} = \left\lceil \sqrt{(M+0.5)/\pi} \right\rceil / f_H \quad (42)$$

which has the dimension of time and helps to normalize the frequency and time arguments as follows:

$$u = \tau f \quad (43)$$

$$\mu = t / \tau \quad (44)$$

With the frequency and time thus-normalized, the soft-spectrum mask can be expanded by the co-basis as

$$P(u) = \sum_{l=0}^{M-1} c_l \phi_l(u) \quad -u_H \leq u \leq u_H \quad (45)$$

where c_l denotes the l th-order expansion coefficient given by

$$\begin{aligned}
 c_l &= \int_{-\infty}^{\infty} \varphi_l(u)P(u)du \\
 &= A \int_{u \in \tau \times I} \varphi_l(u)du - A \int_{u \in \tau \times I_s} \varphi_l(u)du
 \end{aligned}
 \tag{46}$$

where $\tau \times I = [3.1\tau, 10.6\tau]$, representing the τ -scaled UWB band, and $\tau \times I_s$ represents the τ -scaled union of the forbidden sub-bands. Put in matrix form, Eq. (46) means

$$\mathbf{C} = \frac{Au_H}{N} (\mathbf{H}\mathbf{U}^T - \mathbf{H}\mathbf{S}^T)
 \tag{47}$$

where $\mathbf{C} = \{c_l, 0 \leq l \leq M-1\}$ represents a column vector; N is an integer denoting the number of sample points required for numerically calculating the integration, and by rule of thumb, is chosen as $N=2048$ for general DAA functionalities; \mathbf{U} and \mathbf{S} are two N -sampled and unitary-valued row vectors representing the entire UWB band and the forbidden sub-bands respectively; the superscript T denotes the transpose operation; \mathbf{H} is an M by N matrix with its l th row denoting the $(l-1)$ th-order HGFs, which are N -point-sampled on the interval $[-u_H, u_H]$. The waveform of the transmission pulse with normalized time argument is then obtained by applying FRFT to both sides of Eq. (45), namely,

$$p(\mu) = F^{-1}\{P(u)\} = \sum_{l=0}^{M-1} i^l c_l \varphi_l(\mu)
 \tag{48}$$

Finally, the waveform of the transmission pulse $p(t)$ is obtained by de-normalizing the argument μ , that is, by substituting t/τ for μ in Eq. (48), namely

$$p(t) = p(\mu) \Big|_{\mu=t/\tau} = \sum_{l=0}^{M-1} i^l c_l \varphi_l(t/\tau)
 \tag{49}$$

3.6 Implementation of the pulse by Software Defined Radio technique

The pulse given by Eq. (49) involves linear combinations of M τ -scaled HGFs, which are continuous functions. The analogue generation of the pulse is very difficult, whereas the digital generation is much easier. Through modern SDR technique (Reed, 2002), the analogue $p(t)$ can be sampled into a discrete time sequence as

$$p[n] := p(t) \Big|_{t=nT_0} = \sum_{l=0}^{M-1} i^l c_l \varphi_l(nT_0/\tau)
 \tag{50}$$

where $:=$ means sampling. The period of T_0 is determined as follows,

$$T_0 \leq \frac{1}{2f_H}
 \tag{51}$$

In the case of Nyquist sampling, the equality can be used, namely $T_0=1/(2f_H)$; thus, Eq. (50) becomes

$$p[n] = \sum_{l=0}^{M-1} i^l c_l \varphi_l\left(\frac{n}{2u_H}\right)
 \tag{52}$$

where n is defined on the interval equating to $2u_H$ times the support of the co-basis, namely,

$$-2u_H^2 \leq n \leq 2u_H^2 \quad (53)$$

Let $K=4u_H^2$. The length of the resulting sequence $\{p[n], -K/2 \leq n \leq K/2\}$ is then K or $(K+1)$ depending on K being even or odd. Let us take it as K for easy discussion. Putting Eq. (52) in matrix form and denoting $\mathbf{C}=\{c_l, 0 \leq l \leq M-1\}$ where \mathbf{C} is given by Eq. (47), we obtain

$$\mathbf{P} = \frac{Au_H}{N} (\mathbf{U} - \mathbf{S}) \mathbf{H}^T \mathbf{E} \Phi \quad (54)$$

where $\mathbf{P}=\{p[n], -K/2 \leq n \leq K/2\}$ represents the pulse; \mathbf{E} is an M by M diagonal matrix with the diagonal elements $\{e_{ll}\}$ equating to the unitary complex values $\{i^{l-1}, l=1, 2, \dots, M\}$; \mathbf{H} , \mathbf{U} and \mathbf{S} have been defined previously; Φ is an M by K matrix with the l -th row representing the $(l-1)$ th-order scaled-and-discrete HGFs $\phi_l(n/2u_H)$.

We comment that the resultant \mathbf{P} from Eq. (54) is a complex-valued sequence: Its real part is even, known as the inphase part; its imaginary part is odd, known as the quadrature part. In other words, \mathbf{P} is a complex baseband signal, and consequently its generation needs two signal branches (one for the inphase and the other for the quadrature) (Reed, 2002).

3.7 Detection and avoidance scheme

In essence, the pulse \mathbf{P} given by Eq. (54) is a sum of two quantities, each involving a series of matrix multiplications. The matrices \mathbf{H} , \mathbf{E} , and Φ are known *a priori*, keeping unchanged throughout the DAA operation. The row vector \mathbf{U} represents the entire UWB band, keeping also unchanged. Therefore, the minuend in Eq. (54) is a constant sequence, which only needs to be computed once and then stored in the read-only memory (ROM), whereas the row vector \mathbf{S} represents the sub-bands in use by primary users, and it may keep changing under a cognitive environment. Therefore, the subtrahend in Eq. (54) requires to be updated corresponding to the changing radio environment. Obviously, matrix multiplication is a dominant operation. To reduce computation burden, the product $\mathbf{H}^T \mathbf{E} \Phi$ is pre-computed and stored in ROM, so \mathbf{P} only needs to be updated by computing the product of the row vector \mathbf{S} (1 by N) with a matrix $\mathbf{H}^T \mathbf{E} \Phi$ (N by K). Accordingly, the DAA scheme can be devised as follows:

DAA scheme (as illustrated in Fig. 7)

Initialization:

Input A , u_H , N , \mathbf{H} , \mathbf{E} , Φ , and \mathbf{U} .

Compute product $\mathbf{P} = \frac{Au_H}{N} \mathbf{U} \mathbf{H}^T \mathbf{E} \Phi$ and store it in ROM.

Compute and store in ROM the intermediate matrix $\mathbf{I} = \frac{Au_H}{N} \mathbf{H}^T \mathbf{E} \Phi$.

Detecting:

Sense the ambient channel and take samples during some *quiet* period.

Perform FFT computation and multi-taper spectral estimation (Haykin, 2005; Welch, 1967).

Inspect the power emission level and make decision according to a prescribed soft spectrum policy.

If a subband is in use by a primary user(s), mark it as forbidden.

Repeat detecting until the entire UWB band is swept.

Avoiding:

Build row vector S according to the following criteria:

Let the amplitude of the forbidden sub-bands be equal to one.

Let the amplitude of the other sub-bands be equal to zero.

Insert smoothing curves at transitions from one to zero to prevent Gibbs phenomenon.

Compute the instantly changing part $P' = S \times I$.

Update $P = P - P'$.

Output the updated sequence P .

Stop.

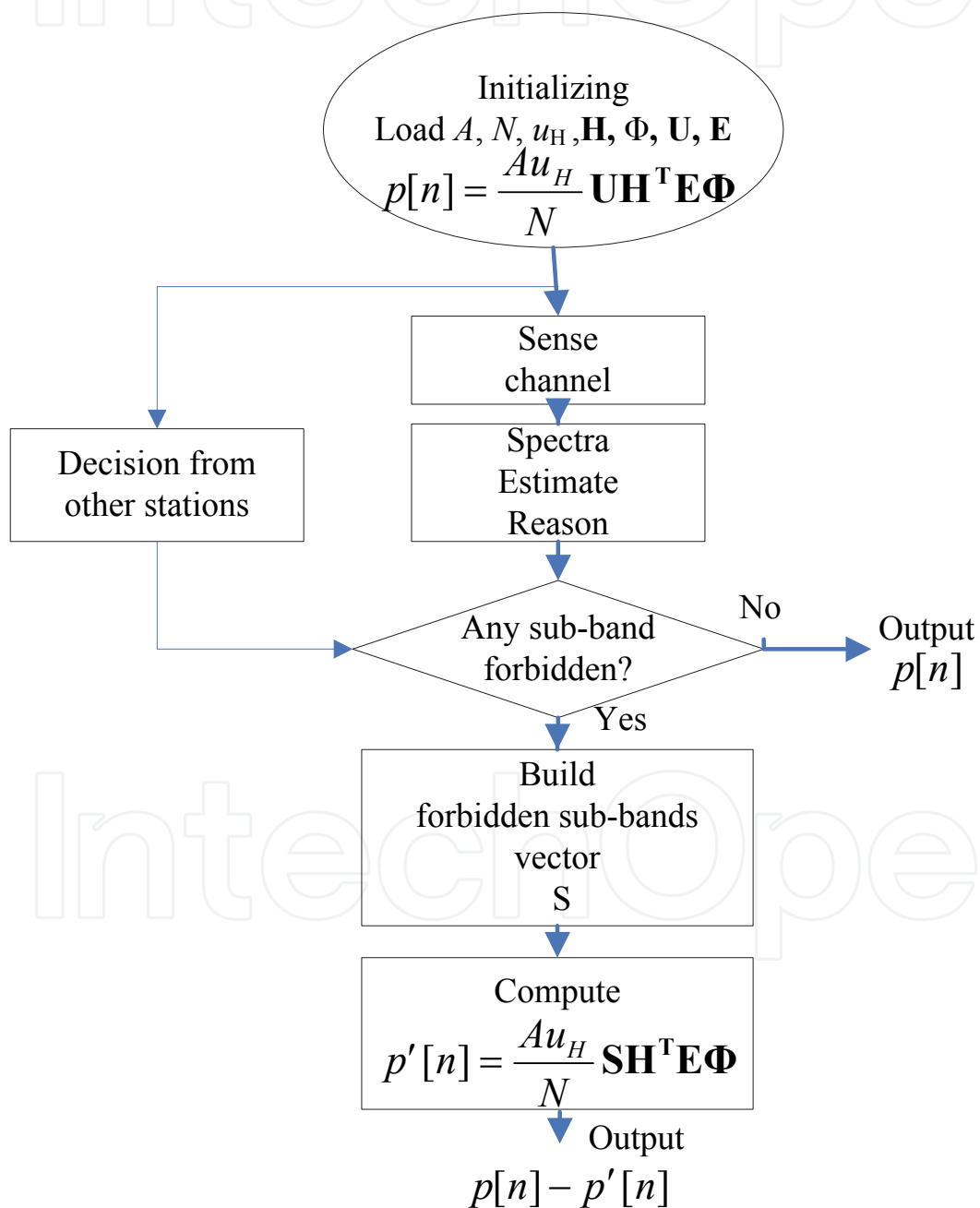


Fig. 7. Flowchart of the DAA Scheme

3.8 Computer simulations

3.8.1 Examples

As examples, we investigate the following two scenarios:

1. No sub-band is in use by primary users; the entire DS-UWB band is accessible.
2. Two sub-bands are in use by primary users: one at central frequency $f_1=4.5$ GHz and the other at $f_2=7.5$ GHz. The bandwidth are both 500 MHz.

The parameters involved are listed in Table 1.

Name	Notation	Typical Values
Lower frequency bound	f_L	3.1 GHz and Below
Upper frequency bound	f_H	10.6 GHz
Chip duration	T_c	10 ns
Amplitude limit	A	2.7×10^{-11} V/Hz
Nyquist sampling period	T_0	0.0472ns
Dimension of the co-basis	M	48
Number of spectrum samples	N	2048
Length of the time sequence	K	64
Normalization factor	τ	0.3774 ns
Interfered central frequencies	f_1	4.5GHz
	f_2	7.5GHz
Bandwidth of the interfered sub-band	Δf	500MHz

Table 1. Basic Parameters involved

For the first scenario, the PSD of the resulting pulse is illustrated in Fig. 8. As expected, the pulse occupies the entire regulated DS-UWB band. Raised-cosine curves have been inserted to smooth the transitional edges of the spectrum vector \mathbf{U} and \mathbf{S} , so the out-of-band ripples are ideally suppressed.

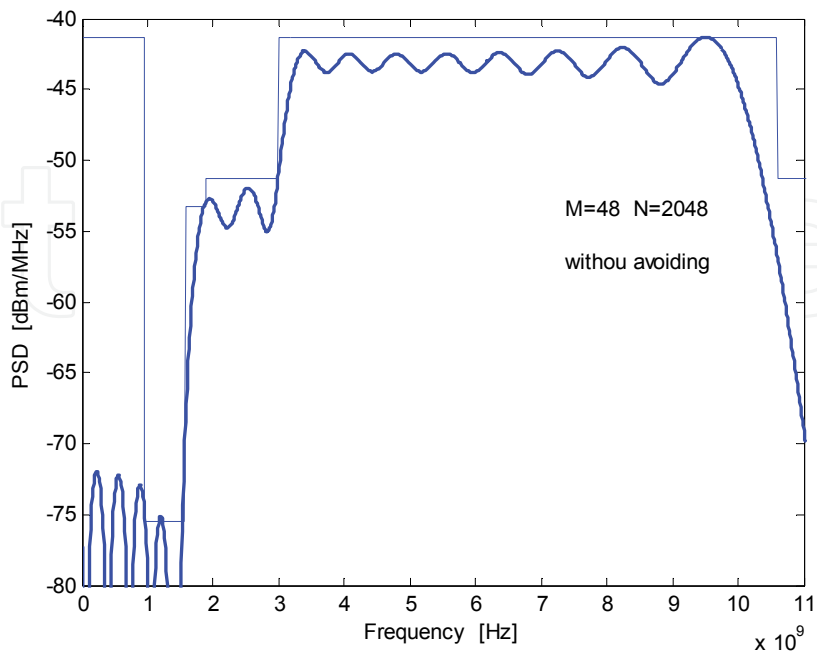


Fig. 8. PSD of the DAA Pulse Using the Entire UWB Band

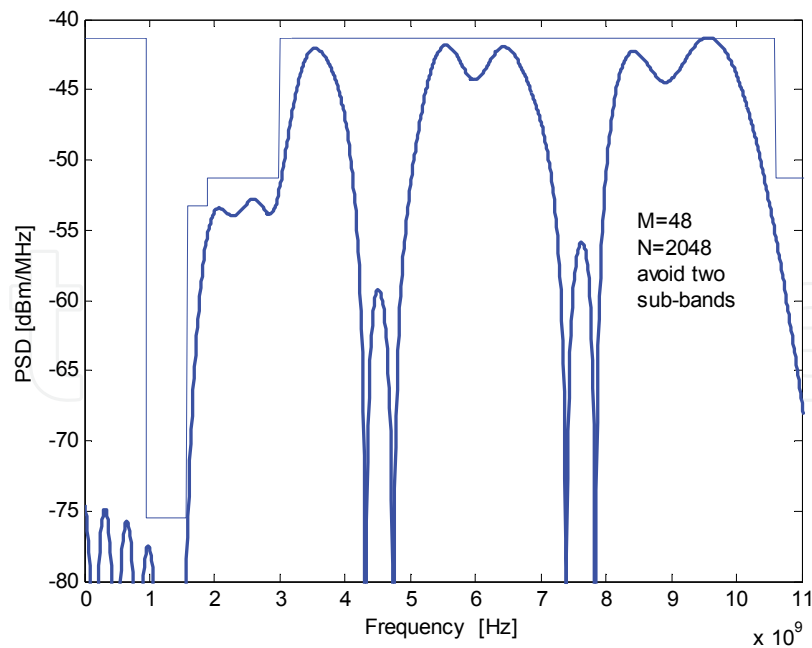


Fig. 9. PSD of the DAA pulse avoiding two sub-bands on which primary users are operating

Fig. 9 illustrates the PSD of the resulting pulse for the second scenario. As expected, the DAA pulse forms two 15dB deep valleys around the two sub-bands in use by the assumed two primary users, effectively avoid interfering the primary users.

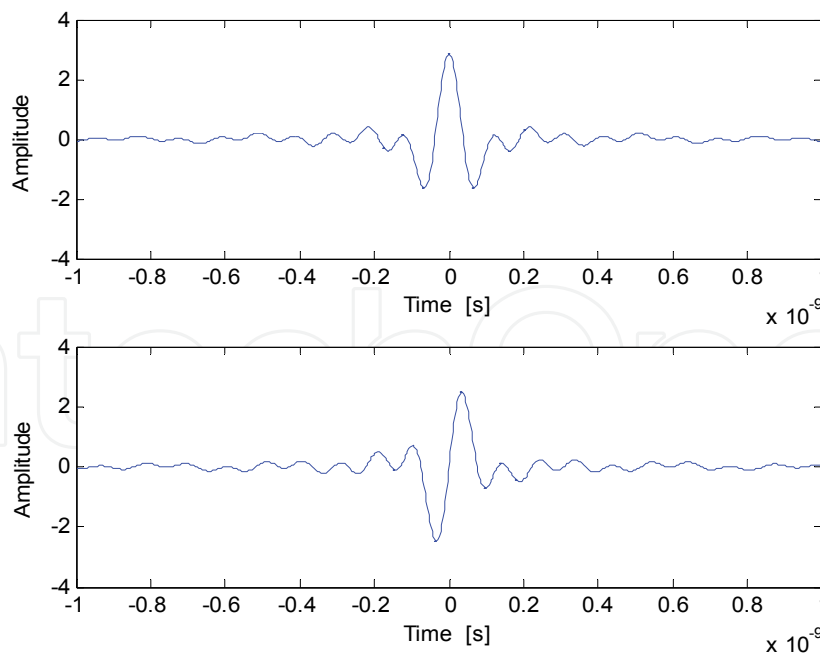


Fig. 10. Waveforms of the DAA Pulse Avoiding Two Sub-bands

The pulse waveforms for the second scenario (for simplicity, the waveforms of the first, which is similar to the second, is left out) is shown in Fig. 10. As seen, the pulse consists of two parts: The real part (on the top) is even, and the imaginary (on the bottom) is odd.

The autocorrelation function, as given by Eq. (32), of the DAA pulse is illustrated in Fig. 11, in which the narrow main-peak suggests that the DAA pulse is sensitive to time jitter, possibly more sensitive than an ordinary pulse, this is the price to pay for DAA.

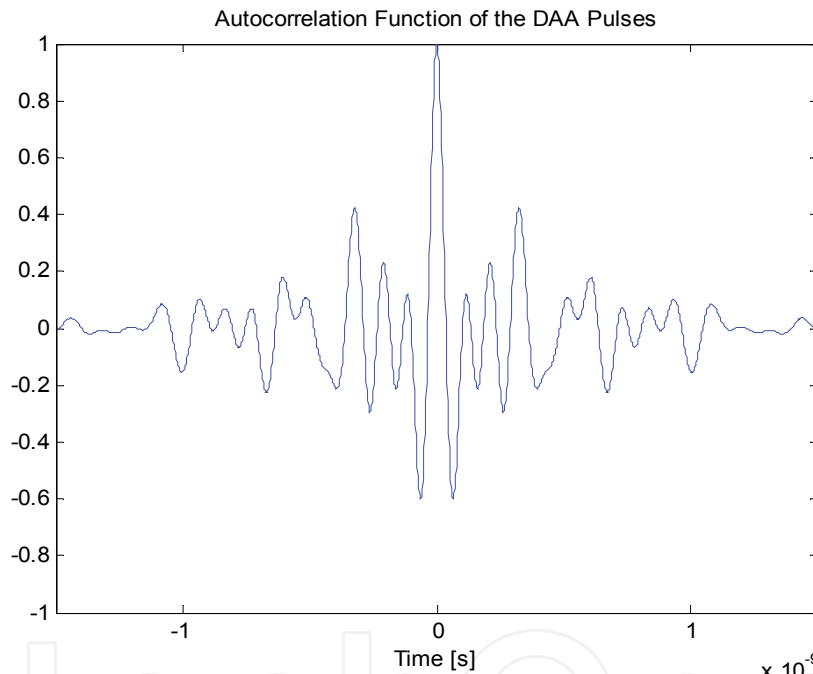


Fig. 11. Autocorrelation Function of the DAA Pulses Avoiding Two sub-bands.

In multi-user or multi-access situations, the DAA pulse works in a similar manner as in a general DS-UWB spread-spectrum scheme. So the performance for multi-user or multi-access under DAA operation is guaranteed by the performance of the pseudorandom or pseudo-noise (PN) sequence assigned for differentiating multi-users. Therefore, the cross-correlation properties of the DAA pulses are out of concern here.

3.8.2 Complexity

The suggested DAA algorithm involves mainly matrix multiplications, for which the dominating operation is complex multiplication. Three factors dictate the total number of multiplications: first, N --the number of sampling points for performing numerical integration; second, M -- the dimension of the co-basis; finally, K --the length of the resulting sequence representing the transmission pulse.

The unchanging part \mathbf{P} requires roughly $K(MN+M+N)$ complex-value multiplications and thus consumes most of the computer time. Given $N=2048$, $M=48$, and the resultant $K=64$, the complex-value multiplications totals 6,425,600 in the simulations. However, the \mathbf{P} only needs to be calculated once, so it does not represent the real computational complexity. On the other hand, the changing part \mathbf{P}' requires to be updated frequently, but its computational time is reduced to NK because the intermediate matrix ($\mathbf{I} = \frac{A_{uH}}{N} \mathbf{H}^T \mathbf{E} \Phi$) has already existed; therefore, the real computational complexity is $\mathcal{O}(NK)$, totaling roughly 131,072, roughly equivalent to 0.1 second if the digital signal processor embedded in the UWB radio operates at one million instructions per second. The amount of time does not vary regardless of the central frequencies and bandwidths of the sub-bands in use by primary users – as opposed to the changeable computational time in the linear combination method addressed in (Benedetto et al., 2004). Therefore, the DAA algorithm has predictable and manageable processing delay, and is robust in real-time communications.

3.9 Conclusion

Detection and avoidance, as a cognitive radio scheme, has been proven effective for multi-band UWB group. The basic idea underlying the DAA is turning off individual carrier-tone on the interfered sub-band. However, coming to direct-sequence UWB, a competing technology group with the multi-band UWB, this idea of turning off tones ceases to be true because shutting off any sub-band would mean to re-design the pulses all over again. In a cognitive environment, the re-design should be agile enough and easily reconfigurable. To this end, we devise a DS-UWB-oriented DAA scheme by emphasizing the side of avoidance (that is, the re-design of the pulse) while de-emphasizing the side of detection by referencing the well-established spectral estimation methods in existing literatures. We propose a domain-less co-basis expansion method in the sense that Hermite-Gaussian functions are used to constitute a common basis (co-basis) for the time and frequency domains. One advantage of the co-basis is that the transmission pulses are directly obtained from the expansion of given soft-spectrum masks, so the resulting pulses fit into arbitrary spectrum masks. Another advantage is that the co-basis functions (that is, the HGFs) are discretized, built as matrices, and stored in ROM, such that whenever a soft spectrum is sensed or discovered, the DAA-enabled pulse is generated by merely matrix multiplying. The amount of computational time is thus trivial, and the re-design of the pulse can respond quickly to a rapidly-changing soft spectrum. The algorithm can be implemented through software defined radio (SDR) techniques.

Computer simulation verifies that the DAA algorithm is low complex, easily configurable, robust, and agile enough to avoid the intended subbands.

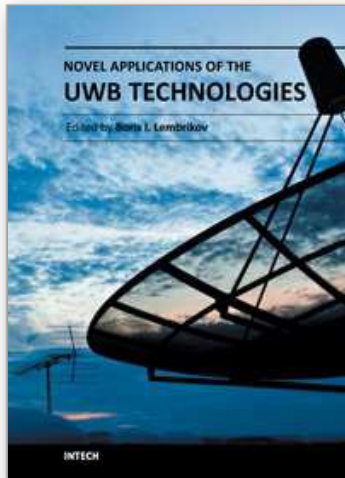
4. References

- Brent Parr et al., "A novel Ultra-Wideband Pulse Design Algorithm," *IEEE Communications letters*, Vol. 7, No. 5, May 2003.
- De, P. & Liang, Y. C. Blind Sensing Algorithms for Cognitive Radio, *Proceedings of 2007 IEEE Radio and Wireless Symposium*, pp. 201-204, Long Beach, USA, January 9-11, 2007
- Dhillon, R. S. & Brown, T. X. Models for Analyzing Cognitive Radio Interference to Wireless Microphones in TV Bands, *IEEE DySPAN 2008*, pp. 1 - 10, Chicago, USA, October 14-17, 2008
- FCC, "Revision of Part 15 of the Commission's Rules Regarding Ultra-wideband Transmission Systems: First Report and Order," *Technical Report FCC 02-48*, 2002.
- Haldun M. Ozaktas et al., *The Fractional Fourier Transform with Applications in Optics and Signal Processing*, John Wiley & Sons, LTD, Chichester, New York, 2000.
- Honggang Zhang & Ryuji Kohno, "Soft-Spectrum Adaptation in UWB Impulse Radio," *the 14th IEEE 2003 International Symposium on Personal, Indoor and Mobile Radio Communication Proceeding*.
- Hu, W. et al. Dynamic Frequency Hopping Communities for Efficient IEEE 802.22 Operation. *IEEE Communications Magazine*, Vol. 45, No. 5, (May 2007), pp. 80-87, ISSN 0163-6804
- IEEE P802.22 working Group for WRAN, Cognitive Wireless RAN Medium Access Control (MAC) and Physical Layer (PHY) specifications: Policies and procedures for operation in the TV Bands, IEEE P802.22/WDv0.4.7 Draft Standard for WRAN Part 22, 2006.
- Jeffrey H. Reed, *Software Radio: A modern Approach to Radio Engineering*, Prentice Hall PTR, 2002.
- Jim Lansford, "UWB Coexistence and Cognitive Radio," *Ultra Wideband Systems 2004*, Joint with Conference on Ultra wideband Systems and Technologies
- John G. Proakis, *Digital Communications, Fourth Edition*, McGraw-Hill Companies, 2003.
- John Walko, "Cognitive Radio," *IEE Review*, [Http://www.iee.org](http://www.iee.org), May 2005.
- Johnstone, I. M. On the distribution of the largest eigenvalue in principle components analysis, *The Annals of Statistics*, Vol. 29, No. 2, (2001), pp. 295-327.
- Kalke, J. TV Band Low Power Devices the need for Coexistence with IEEE 802.22, *IEEE Plenary Tutorial*, pp. 1-10, Vancouver, Canada, November 14-18, 2005
- Lei, Z. D. & Chin, F. A Reliable and Power Efficient Beacon Structure for Cognitive Radio Systems, *IEEE Transactions on Broadcasting*, Vol. 54, No. 2, (June 2008), pp. 182 - 187, ISSN 0018-9316
- Lim, S.; Kim, S.; Park, C. & Song, M. The detection and classification of the Wireless Microphone signal in the IEEE 802.22 WRAN system, *Asia-Pacific Microwave Conference 2007*, pp.1-4, Bangkok, Thailand, December 11-14, 2007

- Maria-Gabriella Di Benedetto et al. (Ed), *UWB Communication Systems: A Comprehensive Overview*, Hindawi Publishing Corporation, 2006.
- Maria-Gabriella Di Benedetto et al., *Understanding Ultra Wide Band Radio Fundamentals*, Prentice Hall PTR, 2004.
- Moe Z. Win. "Ultra-Wide Bandwidth Time-Hopping Spread-Spectrum Impulse Radio for Wireless Multiple-Access Communications," *IEEE Transaction on Communications*, Vol. 48, No. 4, April 2000.
- Mohammad Ghavami et al., "Hermite Function Based Orthogonal Pulses for Ultra Wideband Communications," *Proc. IEEE Wireless Personal Multimedia Conference (WPMC'01)*, Aalborg, Denmark, September 2001.
- Mossa, A. M. & Jeoti, V. Cognitive Radio: Cyclostationarity-Based Classification Approach for Analog TV and Wireless Microphone Signals, *IEEE Innovative Technologies in Intelligent Systems and Industrial Applications 2009*, pp. 107 - 111, Kuala Lumpur, Malaysia, July 25-26, 2009
- Notor, J. The Evolution of Spectrum Sharing in the IEEE 802.22 WRAN Standards Process, http://www.eecs.berkeley.edu/~dtse/3r_notor.ppt, Feb. 2006.
- P. D. Welch, "The Use of Fast Fourier Transform for the Estimation of Power Spectra: A Method base on Time-Averaging over Short, Modified Periodograms," *IEEE Trans. Audio Electroacoustics*, Vol. AU-15, pp. 70-73, 1967.
- Quan, Z.; Cui, S. G.; Poor, H. & Sayed, A. Collaborative wideband sensing for cognitive radios, *IEEE Signal Processing Magazine*, Vol. 25, No. 6, (November 2008), pp. 60 - 73, ISSN 1053-5888
- R. Kohno & K. Takizawa, "Detection and Avoidance Based on Soft-Spectrum Adaptation of UWB Interference to Existing Radio Systems," *IEEE Ninth International Symposium on Spread Spectrum Techniques and Applications*, 2006.
- Rife, D. C. & Boorstyn, R. R. Single Tone Parameter Estimation from Discrete-Time Observations, *IEEE Trans. Inform. Theory*, Vol. IT-20, (September 1974), pp. 591-598, ISSN 1089-7771
- Simon Haykin, "Cognitive Radio: Brain-Empowered Wireless Communications," *IEEE Journal on Selected Areas in Communications*, Vol. 23, No. 2, Feb. 2005.
- Stevenson, C. R. et al. Functional Requirements for the 802.22 WRAN Standard r47, (January 2006)
- Teh, K. C.; Teng, C. C.; Kot, A. C. & Li, K. H. Jammer Suppression in Spread Spectrum, *IEEE Conf. on Information Engineering*, pp. 220-224, 1995.
- Tufts, D. & Kumaresan, R. Singular Value Decomposition and Improved Frequency Estimation Using Linear Prediction, *IEEE Trans. on Acoustics, Speech, and Signal Processing*, Vol. 30, No. 4, (August 1982), pp. 671-675
- Unnikrishnan, J. & Shellhammer, S. Simulation of Eigenvalue based sensing of wireless mics, IEEE 802.22-07/0357r0, (July 2007)
- Wu, Y. C; Wang, H. G. & Zhang, P. Protection of Wireless Microphones in IEEE 802.22 Cognitive Radio Networks, *IEEE International Conference on Communications Workshops 2009*, pp. 1 - 5, Dresden, Germany, June 14-18, 2009

- Zeng, Y. H. & Liang, Y. C. Covariance Based Signal Detections for Cognitive Radio, *Proceedings of 2nd IEEE DySPAN 2007*, pp. 202- 207, Dublin, Ireland, April 17-20, 2007
- Zeng, Y. H. & Liang, Y. C. Eigenvalue-Based Spectrum Sensing Algorithms for Cognitive Radio, *IEEE Transactions on Communications*, Vol. 57, No. 6, (June 2009), pp. 1784 - 1793, ISSN 0090-6778
- Zhenzhen Ye, Madhukumar A. S & Francois Chin, "Power Spectral Density and In-Band Interference Power of UWB Signals at Narrowband Systems," *IEEE International Conference on Communications 2004*, Volume 6, pp. 3561-3565, June 2004.

IntechOpen



Novel Applications of the UWB Technologies

Edited by Dr. Boris Lembrikov

ISBN 978-953-307-324-8

Hard cover, 440 pages

Publisher InTech

Published online 01, August, 2011

Published in print edition August, 2011

Ultra wideband (UWB) communication systems are characterized by high data rates, low cost, multipath immunity, and low power transmission. In 2002, the Federal Communication Commission (FCC) legalized low power UWB emission between 3.1 GHz and 10.6 GHz for indoor communication devices stimulating rapid development of UWB technologies and applications. The proposed book *Novel Applications of the UWB Technologies* consists of 5 parts and 20 chapters concerning the general problems of UWB communication systems, and novel UWB applications in personal area networks (PANs), medicine, radars and localization systems. The book will be interesting for engineers and researchers occupied in the field of UWB technology.

How to reference

In order to correctly reference this scholarly work, feel free to copy and paste the following:

Shaoyi Xu and Rumin Yang (2011). Detection and Avoidance Scheme for DS-UWB System: A Step Towards Cognitive Radio, *Novel Applications of the UWB Technologies*, Dr. Boris Lembrikov (Ed.), ISBN: 978-953-307-324-8, InTech, Available from: <http://www.intechopen.com/books/novel-applications-of-the-uwb-technologies/detection-and-avoidance-scheme-for-ds-uwb-system-a-step-towards-cognitive-radio>

INTECH

open science | open minds

InTech Europe

University Campus STeP Ri
Slavka Krautzeka 83/A
51000 Rijeka, Croatia
Phone: +385 (51) 770 447
Fax: +385 (51) 686 166
www.intechopen.com

InTech China

Unit 405, Office Block, Hotel Equatorial Shanghai
No.65, Yan An Road (West), Shanghai, 200040, China
中国上海市延安西路65号上海国际贵都大饭店办公楼405单元
Phone: +86-21-62489820
Fax: +86-21-62489821

© 2011 The Author(s). Licensee IntechOpen. This chapter is distributed under the terms of the [Creative Commons Attribution-NonCommercial-ShareAlike-3.0 License](#), which permits use, distribution and reproduction for non-commercial purposes, provided the original is properly cited and derivative works building on this content are distributed under the same license.

IntechOpen

IntechOpen